Biotinylated magnetic molecularly imprinted polymer nanoparticles for cancer cell targeting and controlled drug delivery

Maria Nerantzaki, Aude Michel, Laurence Petit, Maylis Garnier, Christine Ménager, Nébéwia Griffete

HAL Id: hal-03648755
https://hal.sorbonne-universite.fr/hal-03648755v1

Submitted on 21 Apr 2022

COMMUNICATION

Biotinylated magnetic molecularly imprinted polymer nanoparticles for cancer cell targeting and controlled drug delivery

Maria Nerantzaki, [*a] Aude Michel,[b] Laurence Petit, [c] Maylis Garnier, [b] Christine Ménager,[b] and Nébéwia Griffete[*b]

Here, multivalent functions have been successfully integrated on a single core-shell type nanostructure, for remote-controlled and receptor-targeted intracellular delivery of doxorubicin (DOX) to breast cancer cells that overexpress biotin receptors.

Breast cancer is the most common malignancy in women worldwide and the second most common cancer overall.[1] In 2020 the World Health Organization declared that 2.3 million women diagnosed with breast cancer and 685 000 dead. Surgical approaches, chemotherapy, hormonal therapies and radiotherapies can all improve breast cancer patients' survival but when applied systemically, these therapies show detrimental side effects due to their lack of tumor targeting specificity and the emergence of tumor multidrug resistance.[2] Hence, an intense emphasis needs to be placed on the development of new technologies that allow targeted destruction of tumours by localizing the delivery of therapeutic agents to the tumour region, while avoiding side-effects.[3-5] Magnetic nanoparticles (MNPs) have enormous potential to overcome these limitations, due to their ability to accumulate in tumors and release anti-neoplastic drugs in response to an external stimulus.

In this framework, polymer-functionalized MNPs based on iron oxide nanoparticles like magnetite (Fe_3O_4) and maghemite (γ-Fe_2O_3), can be safely administered as a colloidal formulation to the human body and other complex model systems, reaching almost any tissue. Additionally, they can generate a localized thermal profile when exposed to an alternating magnetic field (AMF) and can support the loading and release of drugs through physical encapsulation and chemical ligation.[6] In this context, we reported recently the design of a magnetic doxorubicin (DOX) delivery system by growing molecularly imprinted polymers (MIP) from individual iron oxide nanoparticles surface, using different polymerization techniques.[7,8] In such systems the MNPs act as individual "hot spots" and generate acute heat influx when exposed to AMF

which in turn, destabilizes the weak interactions existing between the MIP and the drug, to trigger drug release.

Here, we propose to take advantage of these developments to design novel multifunctional nanovectors, loaded with a cytotoxic anticancer agent such as DOX, directed and guided towards the tumor site and preferentially fixed to the tumor to enhance the destruction of the cells. For this purpose, biotinylated DOX-imprinted MNPs with core-shell morphology have been synthesized and tested *in-vitro* against MCF-7 breast cancer cells. Biotin is an essential vitamin for rapidly dividing cancer cells and as a result, several biotinylated carriers have shown to be able to increase the uptake of anticancer drugs in breast tumor cells.[9] Thus, the proposed magnetic nanomaterial combines the controlled drug release ability of the poly(methacrylic acid) (PMA)-based MIP (under AMF) and the tumor-targeting properties offered by the surface-grafted biotin ligands. Furthermore, in order to ensure the traceability of the system, fluorescent properties have been added by the covalent linkage of acryloxyethyl thiocarbamoyl rhodamine B (RhB), to the polymer backbone of PMA-based MIP coating (Fig.1).

Fig. 1 Schematic representation of the preparation of MIP@DOX-BT MNPs and the concept of AMF-triggered drug delivery system.
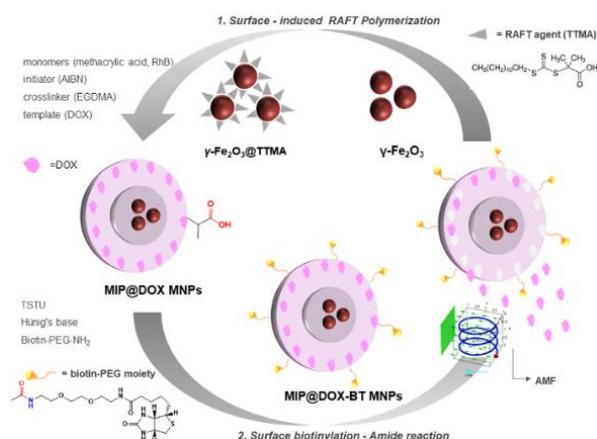
To the best of our knowledge this study will be the first attempt to co-assemble: fluorescent, magnetic, remote-

a. *Université de Strasbourg, CNRS, Institut Charles Sadron UPR22, 23 rue du Loess, 67034 Strasbourg Cedex 2, France*
b. *Sorbonne Université, CNRS, Physico-chimie des Électrolytes et Nanosystèmes Interfaciaux, PHENIX, F-75005 Paris, France.*
c. *IBPS flow cytometry facility, 7 quai Saint Bernard, 75252 Paris Cedex 05*
Electronic Supplementary Information (ESI) availableSee DOI: 10.1039/x0xx00000x

controlled drug release and cancer cell targeting properties in a single core-shell structure. Thus, we believe that it will be a major advance in the development of multifunctional targeted drug delivery nanotechnologies. In our first reports, we demonstrated that the surface-induced reversible addition-fragmentation chain-transfer (RAFT) polymerization technique is a practical grafting-from approach to develop advanced stimuli responsive magnetic MIPs for drug delivery applications.[7,8] Here, in order to obtain surface-imprinted MNPs with uniform core-shell structure and breast cancer targeting properties, we modified the polymerization conditions and added a post-polymerization functionalization step.

As it is illustrated in Figure 1, initially, the outer surface of γ-Fe_2O_3, prepared via a chemical co-precipitation method, was functionalized by a chain transfer agent (2-(dodecylthiocarbonothioylthio)-2-methylpropionic acid (TTMA) via non-covalent electrostatic interactions. Second, a fluorescent PMA-co-RhB DOX-imprinted polymer layer was grown from the surfaces of MNPs via RAFT polymerization, using DOX as template, methacrylic acid (MA) and acryloxyethyl thiocarbamoyl rhodamine B (1.5 mol % relative to MA), as (co)monomers, in the presence of ethylene glycol dimethylacrylate (EGDMA) and azobisisobutyronitrile (AIBN), as crosslinker and initiator, respectively. Even if DOX is fluorescent, we added Rhodamine B into the materials for biological experiments to acutely follow the targeting of the materials to the cells, as the DOX concentration encapsulated in the material could be low. Then, the covalent attachment of poly(ethyleneglycol)amine (BT-PEG-NH_2) ligands to the MIP@DOX nanoparticles surface was performed by amide bound formation.[10-12] A detailed description of the TSTU-mediated amide coupling of biotin-poly(ethyleneglycol)amine (BT-PEG-NH_2) ligands on the surface of MIP@DOX nanoparticles is given in Fig. 1 and Fig. SI1.

Transmission electron microscopy (TEM) images of MIP@DOX-BT sample (Fig.2a) demonstrate that nanoparticle sizes range between 30 and 60 nm (Fig. 2c). The particles showed a roughly spherical morphology, with uniform core-shell structure. Higher magnification TEM image (Fig. 2b) indicates that MIP@DOX-BT MNPs are composed of one to four magnetic cores, surrounded by a uniform polymeric shell of 20 nm. The presence of the polymer shell is also evidenced by dynamic light scattering (DLS) measurements. More particularly, the DLS measurements showed an increase of the hydrodynamic diameter of the bare MNPs (D_H = 17nm) after surface modification with TTMA (D_H = 28nm) and after polymerization (D_H = 52 nm). In addition, DLS results indicated that the synthesized MIP@DOX-BT sample has a narrow size of 67nm with a polydispersity index (PDI) of 0.2. Ultimately, DLS analysis is in good agreement with TEM measurements and reveals that MIP@DOX-BT MNPs can be synthesized with controlled composition, shape, size and morphology.

Shape and nanoparticle size together with chemical composition, are crucial parameters in cellular uptake.[13] An ideal delivery system has a size ranging from 30 to 300 nm, with the possibility of being more finely tuned for the specific application under consideration. Owing to their small size and spherical shape MIP@DOX-BT MNPs are expected to undergo cellular internalization rapidly and efficiently. Apart from internalization, with a diameter of 53 nm MIP@DOX-BT MNPs hold a great promise for prolonged blood circulation. Polymeric nanoparticles smaller than 10 nm are directly excreted by kidneys, while sizes larger than 300 nm should be avoided due to problems such as thrombosis and rapid elimination through liver and spleen.[14, 15]

The chemical composition of MIP@DOX-BT MNPs was studied by Fourier transform infrared (FTIR) spectroscopy. The FTIR spectra of the as-synthesized nanoparticles before (MIP@DOX) and after biotinylation (MIP@DOX-BT) are presented in Fig. 2d, together with the spectra of bare (γ-Fe_2O_3) and modified (Fe_2O_3@TTMA) MNPs. The spectra of all samples show a strong peak around 583 cm^{-1} which is related to the vibration of the Fe- O group and a broad band in the region between 3500 and 3800 cm^{-1}, which is assigned to the surface-absorbed water and hydroxyl groups.[16] In the spectrum of Fe_2O_3@TTMA MNPs, the peaks occurring at 2952 cm^{-1} can be associated with the bending and stretching of C-H in TTMA (Fig. SI2a). Moreover, the presence of a PMA-based MIP shell in MIP@DOX MNPs is confirmed by FTIR spectroscopy, since the characteristic stretching vibration peak of the C=O group was recorded at 1636 cm^{-1} (Fig. SI2b). The successful attachment of BT-PEG-NH_2 ligands to the PMA-based MIP layer of MIP@DOX-BT MNPs is also evidenced by FTIR, as new peaks emerged compared to particles before the amide coupling. More particularly, the characteristic bands of amide I (due to C=O stretching vibration) and amide II (caused by NH_2 deformation) were detected at 1710 cm^{-1} and 1450 cm^{-1}, respectively.[17] For a quantitative determination of DOX encapsulated in the MIP@DOX-BT MNPs, we performed UV-visible analysis of the particles, of DOX and determined a concentration of 11.5µM of DOX/g of particles (Fig. SI3) in agreement with the DOX quantified in the supernatants after the synthesis (12µM of DOX).

Thermogravimetric analysis (TGA) curves of MIP@DOX MNPs and MIP@DOX-BT MNPs are shown together with the curves of bare γ-Fe_2O_3 MNPs and Fe_2O_3@TTMA MNPs (Fig. 2d). In brief, the initial loss of moisture between 65-170°C is followed by a significant mass loss between 280–390°C, resulting from the decomposition of organic matter.

Fig. 2 a, b) TEM images after negative staining of MIP@DOX-BT MNPs at low and high magnification, c) histogram for size distribution by TEM image analysis, d) FTIR spectra and e) TGA curves of Fe_2O_3, Fe_2O_3@TTMA, MIP@DOX and MIP@DOX-BT MNPs.
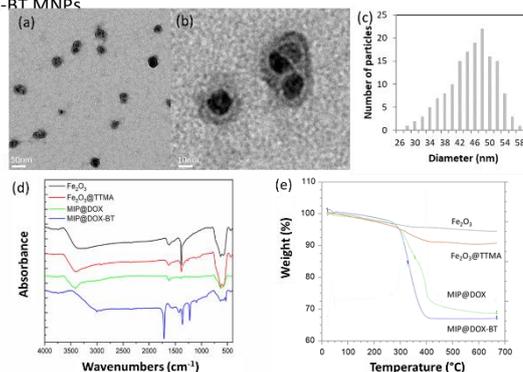
Above 390 °C TGA curves slow down to complete the degradation of the organic matter until a constant mass is reached.[18] The constant mass remaining at the end of each TGA experiment corresponds to γ-Fe$_2$O$_3$ MNPs. The TGA curve of Fe$_2$O$_3$@TTMA MNPs showed a mass loss of 10% attributed to the organic compounds of TTMA, while for the MIP@DOX and MIP@DOX-BT samples the maximum weight loss increased from 68 to 70 % with the increase of organic matter content.

To demonstrate the presence of functional BT on the surface of MIP@DOX-BT MNPs, we used the avidin/HABA (2-Hydroxyazobenzen-4'-Carboxylic Acid) colorimetric assay developed by Green as HABA, can be stoichiometrically displaced by biotin.[19] Fig. SI4 presents the UV–visible spectra of the avidin/HABA complex before and after the addition MIP@DOX and MIP@DOX-BT MNPs. As the absorbance of the avidin/HABA complex at 500 nm decreased upon the addition of the MIP@DOX-BT, we concluded that BT bound to HABA as a result of its higher affinity for avidin (Ka=10^{-15}M^{-1}). Based on Beer–Lambert law (Fig. SI5) we obtain the biotin concentration of the MIP@DOX-BT solution (C=5.3 nmol.ml^{-1}). This subsequently leads to the biotin-binding capacity of the MIP@DOX-BT MNPs which was found to be 2.6 nmol mg^{-1}. The small decrease for MIP@DOX sample can be attributed to nonspecific interactions between the avidin/HABA complex and the non-functionalized MNPs (0.6 nmol. mg^{-1}). Consequently, MIP@DOX-BT MNPs with unique properties and well-defined structure were obtained by using surface-induced RAFT molecular imprinting technique, followed by TSTU-mediated amide coupling.

In order to assess the efficacy of MIP@DOX-BT MNPs as magnetic hyperthermia source, the specific loss power (SLP, in W.g^{-1} of iron) was estimated to 24 W.g^{-1} at 335 kHz and 9mT magnetic field in PBS (Fig. SI6). Then, we looked at the *in vitro* doxorubicin release of MIP@DOX-BT MNPs in PBS. The sample ([Fe]=5mM) was periodically placed under AMF and the particles released 9.3 µM of DOX after 4h at 37°C (Fig. SI7b) whereas a sample left for 4h at 37°C did not show any significant DOX release (1µM, Fig. SI7a).

Targeting tests of MCF-7 cells were performed by controlling the adsorption of fluorescent MIP@DOX-BT MNPs on the surface of the cells using two different techniques: confocal microscopy in order to image the fluorescent of particles and flow cytometry in order to obtain the cell percent that are fluorescent. Indeed, as the nature of the polymer can induce non-specific adsorption of proteins, it is necessary to determine the efficiency of the imprinting process and the specificity of the targeting using fluorescent MIP@DOX MNPs as control. Considering this, MCF-7 cells were first incubated for 1 hour with MIP@DOX and MIP@DOX-BT MNPs at fixed iron concentration ([Fe] = 5 mmol.L^{-1}, [DOX] = 12.5 µmol.L^{-1}) at 37°C. As we can see on Fig. 3 (and Fig. SI8), the marked cells percent, evaluated using flow cytometry, is high for both type of particles, MIP@DOX (B) and MIP@DOX-BT (C), when looking at RhB (42.2 and 73.8 %) or DOX fluorescence (10.8 and 24.9 %) and the control cells (A) are not fluorescent.
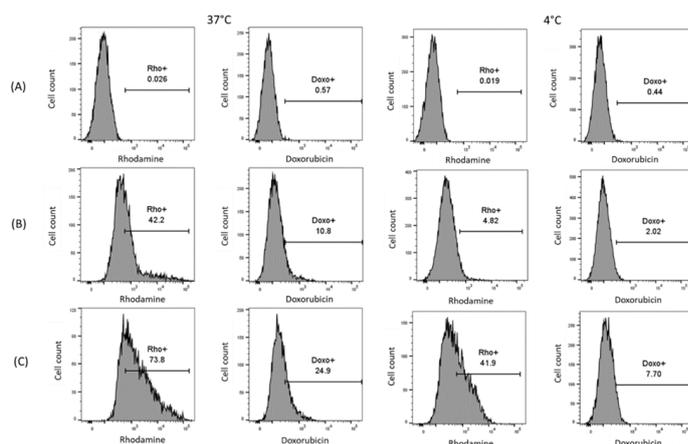

Fig.3 Flow cytometry measurements of the fluorescence intensity distributions of MCF-7 breast cancer cells incubated with (B) MIP@DOX or (C) MIP@DOX-BT at 4°C and 37°C. Cells without particles were used as a control (A). The excitation wavelength was at 561nm for rhodamine B and the fluorescence was collected through the band-pass of 579/593 nm; the excitation wavelength for doxorubicin was at 488nm and the fluorescence was collected through the band-pass of 589/639 nm. The horizontal axis represents the fluorescence intensity.

At 37°C the particles enter into the cells by endocytosis even if they are not modified with a BT ligand. Hence, to observe only the NPs adsorbed on the cell membrane, the endocytosis was blocked by incubating the particles at 4 °C and we only detect the fluorescence intensity of the particles adsorbed on the surface of the cells. Based on the results demonstrated in Fig. 3 (and Fig. SI8), the marked cells percent in the rhodamine B and doxorubicin channel for the cells incubated with (C) biotynilated particles (respectively 41.9 and 7.7%) is higher than (B) without this ligand (4.82 and 2.02%). This result proves the efficient targeting of the MCF-7 presenting BT receptors at its surface cells when biotin ligands are grafted at the surface of MIP@DOX MNPs.

The targeting efficiency of the nanoparticles were then tracked by confocal microscopy (Fig. SI9). The images were taken 2 h after the incubation at 37 and 4°C. When cells are incubated with MIP@DOX and MIP@DOX-BT MNPs at 37°C, the particles (in red) appears localized in the cytoplasm of the cells. When the incubation is performed at 4°C, the particles appear localized at the surface of the cells. Besides, this fluorescence is higher for the biotinylated nanoparticles in agreement with flow cytometry results.

Then we looked at the cell viability of MCF-7 incubated with the particles (Fig. 4A) in order to determine if we can decrease the cell viability when using particles that can target these cells. First, MIP@DOX and MIP@DOX-BT MNPs internalization do not induce cancer cell death (green and blue on Fig. 4A), demonstrating that the hybrid nanomaterials synthesized are not toxic. It thus evidences that DOX is well sequestered within the MIP, therefore inactive in terms of cytotoxicity. After AMF application (90min at 335 kHz, 9 MT), to the cancer cell containing MIP@DOX, the cell viability is reduced from 88 to 78 %. When applying the AMF to the cancer cells containing MIP@DOX-BT, the viability is highly affected with a cell
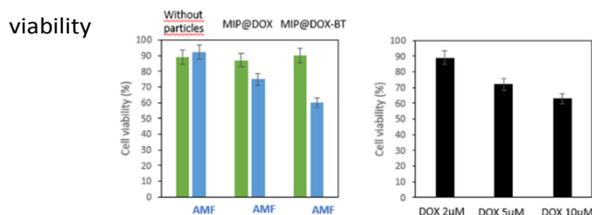
viability

reduced from 90 to 60%. We previously showed that under AMF

Fig.4 (A) MCF-7 cancer cells metabolic activity (cell viability) without particles (control), in presence of MIP@DOX and MIP@DOX-BT MNPs without and with AMF (B) with different concentration of free DOX (2, 5 and 10 µM).

the drug goes into the nucleus after AMF application leading to the cancer cell viability decrease.[8] Moreover, during all the cell experiments, the temperature did not increase (Fig. SI10) demonstrating that the reduction of the cell viability is due to the drug release and not to a macroscopic heating of the medium. Hence, if we use magnetic particles that can specifically target the desire cells, we can increase their internalization and decrease the cell viability under AMF for the incubation of the cells with different concentration of free DOX (2, 5 and 10 µM), decreases. These results agree with the initial concentration of DOX encapsulated in the MIP (12.5µM for a concentration of iron of 5mM).

Consequently, the adverse effects of chemotherapy on healthy tissues could be reduced by using MIP@DOX-BT MNPs. Yet, to apply these nanocarriers into the cancer treatment, many fundamental questions on their biocompatibility and long-term fate in biological environments still need to be addressed.[15,20] Although, there are several examples indicating that polymethacrylate nanoMIPs are not toxic, studies on the toxicity and clearance mechanism of MIP-coated iron oxide MNPs are almost nonexistent.[21,22] We recently showed that the polymethacrylate-based MIP coating on the surface of magnetic iron oxide nanoparticles are not toxic and we studied the degradation of the inorganic core. We showed that the polymer is degraded in spheroids, but of course further study should be performed to explore the behavior of the MIP.[23] We can expect that MIP@DOX-BT MNPs are still not cytotoxic at least *in vitro*.

Conclusions

To conclude, we developed magnetic core-shell type nanoparticles (MIP@DOX-BT MNPs) with specific cell targeting as well as controlled drug release properties, by using a simple and efficient synthetic strategy. The nanocarriers consist of magnetic multi-cores covered with a biotin-functionalized DOX-loaded MIP shell. Due to these unique features, they are capable of targeting MCF-7 cells *in vitro*, while keeping the cytotoxic drug without any passive drug release. Upon AMF, the drug is released due to local heating of the magnetic cores leading to the disruption of hydrogen bonding existing between the MIP and the drug. Interestingly, when the nanoparticles possess a targeting molecule, the cell viability is widely decreased compared to the same magnetic material but without the targeting. The results from this study are promising and open up interesting avenues for future research on targeted therapy drugs for other cancer cell types. Nevertheless, continuing efforts to fundamentally understand clearance and tumor targeting of this material, so that it can be translated into the clinical practices.

Conflicts of interest

''There are no conflicts to declare''.

Acknowledgements

References

1. N. Harbeck, F. Penault-Llorca, J. Cortes, M. Gnant, N. Houssami, P. Poortmans, K. Ruddy, J. Tsang and F. Cardoso, *Nature Reviews Disease Primers*, 2019, **5**, 66.
2. A. G. Waks and E. P. Winer, *Jama*, 2019, **321**, 288.
3. A. Bhushan, A. Gonsalves and J. U. Menon, *Pharmaceutics*, 2021, **13**, 723.
4. A. S. Perera, S. Zhang, S. Homer-Vanniasinkam, M. O. Coppens, M. Edirisinghe, *ACS Appl. Mater. Interfaces*, 2018, **10**, 15524.
5. A. T. Paulino, A. G. B. Pereira, A. R. Fajardo, K. Erickson, M. J. Kipper, E. C. Muniz, L. A. Belfiore, E. B. Tambourgi *Carbohydrate Polymers*, 2012, **3**, 1216.
6. E. Cazares-Cortes, S. Cabana, C. Boitard, E. Nehlig, N. Griffete, J. Fresnais, C. Wilhelm, A. Abou-Hassan and C. Ménager, *Advanced Drug Delivery Reviews*, 2019, **138**, 233.
7. N. Griffete, J. Fresnais, A. Espinosa, C. Wilhelm, A. Bée and C. Ménager, *Nanoscale*, 2015, **7**, 18891.
8. M. Nerantzaki, A. Michel, E. Briot, J. M. Siaugue, C. Ménager, C. Wilhelm and N. Griffete, *Chemical Communications*, 2020, **56**, 10255.
9. K. Vinothini, N. K. Rajendran, M. A. Munusamy, A. A. Alarfaj and M. Rajan, *Mater Sci Eng C Mater Biol Appl*, 2019, **100**, 676.
10. E. Massolo, M. Pirola and M. Benaglia, *European Journal of Organic Chemistry*, 2020, **2020**, 4641.
11. S. Y. Kim, S. H. Cho, Y. M. Lee and L.-Y. Chu, *Macromolecular Research*, 2007, **15**, 646.
12. E. Valeur and M. Bradley, *Chem. Soc. Rev.* , 2009, **38**, 606.
13. S. Behzadi, V. Serpooshan, W. Tao, M. A. Hamaly, M. Y. Alkawareek, E. C. Dreaden, D. Brown, A. M. Alkilany, O. C. Farokhzad and M. Mahmoudi, *Chemical Society Reviews*, 2017, **46**, 4218.
14. J. Lazarovits, Y. Y. Chen, E. A. Sykes and W. C. W. Chan, *Chemical Communications*, 2015, **51**, 2756.
15. R. Ferrari, M. Sponchioni, M. Morbidelli and D. Moscatelli, *Nanoscale*, 2018, **10**, 22701.
16. M. Nazari, N. Ghasemi, H. Maddah and M. M. Motlagh, *Journal of*

Nanostructure in Chemistry, 2014, **4**, 99.

17. Y. Ji, X. Yang, Z. Ji, L. Zhu, N. Ma, D. Chen, X. Jia, J. Tang and Y. Cao, *ACS Omega*, 2020, **5**, 8572.

18. G. Kandasamy, S. Surendran, A. Chakrabarty, S. N. Kale and D. Maity, *RSC Advances*, 2016, **6**, 99948.

19. N. M. Green, *Biochem J*, 1965, **94**, 23c-24c.

20. K. G. Shevchenko, I. S. Garkushina, F. Canfarotta, S. A. Piletsky and N. A. Barlev, *RSC Advances*, 2022, **12**, 3957.

21. M. Gagliardi, A. Bertero and A. Bifone, *Scientific Reports*, 2017, **7**, 40046.

22. S. Farzaneh, E. Asadi, M. Abdouss, A. Barghi-Lish, S. Azodi-Deilami, H. A. Khonakdar and M. Gharghabi, *RSC Advances*, 2015, **5**, 9154.

23. C. Boitard, A. Curcio, A.-L. Rollet, C. Wilhelm, C. Ménager and N. Griffete, *ACS Applied Materials & Interfaces*, 2019, **11**, 35556-35565.